


Investigation of Mo-, Pt-, and Rh-doped rutile TiO₂ based on first-principles calculations

Cite as: AIP Advances **8**, 075014 (2018); <https://doi.org/10.1063/1.5038776>

Submitted: 05 May 2018 . Accepted: 05 July 2018 . Published Online: 16 July 2018

Xuefeng Lu , Tingting Zhao, Xu Gao, Junqiang Ren, Xiaobin Yan, and Peiqing La



View Online



Export Citation



CrossMark

ARTICLES YOU MAY BE INTERESTED IN

[Fabrication and characterization of superconducting MgB₂ thin film on graphene](#)

AIP Advances **8**, 075015 (2018); <https://doi.org/10.1063/1.5023658>

[A review on applications of Cu₂ZnSnS₄ as alternative counter electrodes in dye-sensitized solar cells](#)

AIP Advances **8**, 070701 (2018); <https://doi.org/10.1063/1.5038854>

[Combined I\(V\) and dI\(V\)/dz scanning tunneling spectroscopy](#)

AIP Advances **8**, 075013 (2018); <https://doi.org/10.1063/1.5034422>



NEW

AVS Quantum Science

A high impact interdisciplinary journal for **ALL** quantum science

ACCEPTING SUBMISSIONS



Investigation of Mo-, Pt-, and Rh-doped rutile TiO₂ based on first-principles calculations

Xuefeng Lu,^a Tingting Zhao, Xu Gao, Junqiang Ren, Xiaobin Yan, and Peiqing La

State Key Laboratory of Advanced Processing and Recycling of Non-Ferrous Metal, Department of Materials Science and Engineering, Lanzhou University of Technology, Lanzhou 730050, PR China

(Received 5 May 2018; accepted 5 July 2018; published online 16 July 2018)

In the present research, we use a first principles calculation to investigate the electronic structure and optical properties of Mo-, Pt- and Rh-doped rutile TiO₂. The results indicate that the band gap of the Mo-, Pt-, and Rh-doped systems decreases to 1.758, 0.906, and 0.971 eV, respectively, compared with the 1.968 eV band gap of intrinsic TiO₂, which is due to the hybridization of the doped atom *d* and O *p* orbital electrons, resulting in the formation of an impurity level and enhanced conductivity. The charge-difference density maps show that the covalence is enhanced in the region around Ti atoms for Mo- and Pt-doped systems, whereas Rh doping has little effect on the covalence. Based on these results, the bond population is 0.42, 0.28, and 0.27 for Mo–O, Pt–O, and Rh–O bonds, respectively. In the absorption spectrum, the peaks of the doped systems decrease significantly and redshift. Compared with the Mo-doped system, the Rh- and Pt-doped systems have lower static dielectric constant and dielectric loss in the low-energy region, which is promising for fascinating applications in microelectronic components. © 2018 Author(s). All article content, except where otherwise noted, is licensed under a Creative Commons Attribution (CC BY) license (<http://creativecommons.org/licenses/by/4.0/>). <https://doi.org/10.1063/1.5038776>

I. INTRODUCTION

Titanium oxide, commonly known as titanium dioxide, is a white inorganic pigment and is nontoxic, nonhazardous, has high chemical stability, excellent opacity, excellent whiteness and gloss, and the highest shading coefficient. As such, it is currently considered as one of the best white pigments available. It is a wide-bandgap semiconductor, and typically comes in three forms: the anatase phase, rutile phase, and brookite phase, with the first two phases being the most common. Recently, due to its excellent optical, electrical, magnetic, and electrochemical properties, it has been the subject of extensive theoretical and experimental research¹ in the fields of photoelectric^{2,3} catalysis^{4,5} and solar cells.⁶ This work has shown that the band gap of the pure anatase phase TiO₂ is about 3.23 eV,^{1,7,8} which results in a significant reduction in the absorption efficiency of solar energy, therefore requiring performance improvement. Doping is reported to be an effective method to reduce the band gap of TiO₂,^{7–9} so the exploration of doped TiO₂ systems has become a top priority in current research.

Numerous previous studies have looked at various doping strategies of anatase TiO₂. Through experiments with La-doped TiO₂ nanotubes, Xue et al.¹ concluded that the photocatalytic performance of TiO₂ nanotubes increases with increasing La doping content for a mass fraction of less than 1%; excessive doping (>1%) leads to a decrease in the photocatalytic performance. For W-S codoped anatase TiO₂, Wu et al.⁷ found that the band gap of S-doped TiO₂ decreases and, simultaneously, a shallow acceptor level is introduced at the top of the valence band, thereby reducing the energy required for electrons to transition from the valence band to the conduction band. This leads to a

^aCorresponding author: Tel: +086-13919962508; Fax: +086-09312976725; E-Mail: luxuefeng1979@163.com



redshift of the absorption spectrum and increased photocatalytic activity under visible-light excitation. Wang *et al.*⁸ concluded that the hybridization of the C 2*p*, Zn 3*d*, Ti 3*d*, and O 2*p* orbital electrons leads to the formation of new impurity levels between the conduction band and the valence band. These impurity levels occur near the Fermi level and reduce the band gap, which is conducive for the diffusion of photogenerated carriers in the crystal, thereby improving the photocatalytic performance. In addition, Xu *et al.*⁹ found that Ti 3*d* orbital electrons move to N 2*p* orbits, which causes the entire conduction band to move towards the Fermi level, thus narrowing the band gap of TiO₂. Pan *et al.*¹⁰ found that an impurity level is introduced in rutile TiO₂ upon doping with C and mainly forms the coupling of the O 2*p* and C 2*p* orbitals. In addition, the introduction of impurity levels can increase the response to visible light, thus increasing the absorption range of TiO₂. Overall, the formation of impurity levels derived from the *d* orbital of the dopants and the *p* orbital of bulk atoms is possible and is very effective for reducing the band gap of TiO₂.

Many studies have recently investigated changing the band gap of the anatase TiO₂ by doping. Unfortunately, during such experiments, anatase TiO₂ forms a complex phase with the rutile phase TiO₂. Reports on how to reduce the band gap of rutile TiO₂ are lacking, making it increasingly difficult to change the band gap of the compound. Therefore, the present work looks at modifying rutile TiO₂ by reducing its band gap through doping and then investigating the optical properties of the doped system. This work provides a theoretical basis and experimental directions for doping anatase TiO₂ and rutile TiO₂ compound. We use Mo, Pt, and Rh as dopants because their radii are very close to that of Ti, thereby minimizing any lattice distortion after doping. At the same time, the three dopants possess abundant *d* orbital electrons, which are beneficial for forming impurity energy levels from the dopant *d* orbital and the *p* orbitals of bulk atoms, thereby reducing the band gap of the system.

II. MODEL AND COMPUTATIONAL METHOD

The model is established and the calculation is done within density functional theory by using the plane-wave pseudopotential method, as implemented in the CASTEP code. The space group of

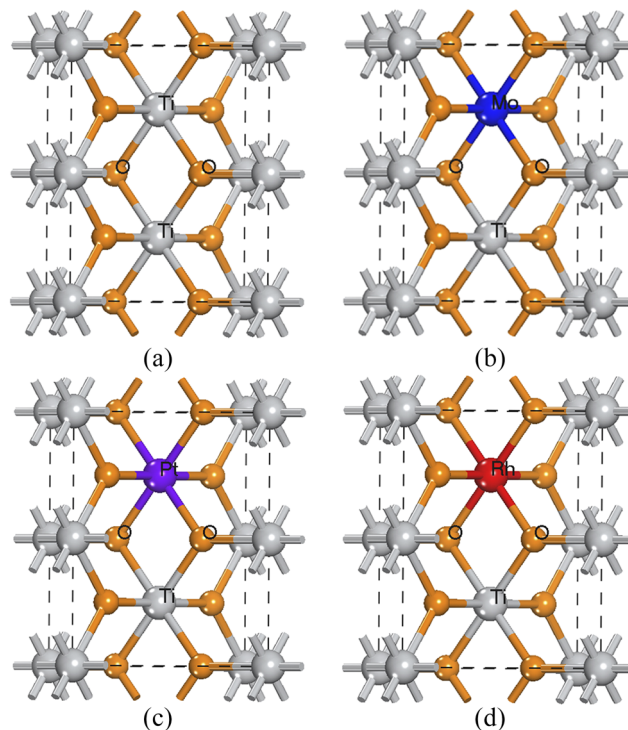


FIG. 1. Models of $1\times 1\times 2$ supercell of free and doped rutile TiO₂: (a) undoped, (b) Mo doped, (c) Pt doped, (d) Rh doped.

rutile TiO_2 is $P42/mnm$, making it a tetragonal system. A Ti atom is located at the center of the crystal lattice and six O atoms are located at the corners of the octahedron, with each octahedron connected to ten surrounding octahedral bodies.¹¹ On this basis, we set up the $1 \times 1 \times 2$ supercell, and then replace one Ti atom with either a Mo, Pt, or Rh atom, as shown in Fig. 1. In the optimization process, the exchange-correlation energy is described by using the generalized gradient approximation in the scheme of Perdew-Burke-Ernzerhof. In addition, since the plane-wave cutoff energy strongly affects the optimization, the cutoff energy is set at 400 eV, which is higher than the cutoff energy in the literature.^{7,8} The energy convergence standard is set to 2×10^{-6} eV/atom, the maximum displacement is 5×10^{-5} nm, the maximum stress is 0.01 eV, the internal stress of the crystal does not exceed 0.02 GPa, and a k point mesh is used with a $4 \times 4 \times 1$ grid in the irreducible part of the Brillouin zone. After geometric optimization, all parameters are within the convergence range. Ti $3d^2 4s^2$, O $2s^2 2p^4$, Mo $4d^5 5s^1$, Pt $5d^9 6s^1$, and Rh $4d^8 5s^1$ are included as valence electrons, and all calculations are done in reciprocal space.

III. RESULTS AND DISCUSSION

A. Geometry optimization

Table I gives the lattice parameters after geometric optimization of the supercell. The lattice constants of the supercell are $a = 4.675 \text{ \AA}$ and $2c = 5.925 \text{ \AA}$ after optimizing the pure rutile TiO_2 supercell. These results are consistent with the experimental values $a = 4.594 \text{ \AA}$ and $2c = 5.917 \text{ \AA}$ ¹⁰ and the calculated values $a = 4.665 \text{ \AA}$, $2c = 5.947 \text{ \AA}$,¹¹ indicating that the proposed model is reliable. Simultaneously, the pure supercell and the doped supercell have similar volumes, and the change of the crystal constant is not obvious, indicating that the doping causes little lattice distortion, which is very favorable for maintaining the stability of the system.

B. Structure of energy band

The stability of the doping system can be described by the crystal-formation energy, with smaller formation energy corresponding to a more stable crystal structure.¹² Figure 2 shows the calculated band gap, total energy, and formation energy. The results show that the Mo-doped system has a total energy of -10255.822 eV and a formation energy of 3.099 eV, which are less than other doping systems, implying that the stability of the Mo-doped system is the best of the three doped systems. Furthermore, the band gap of pure rutile TiO_2 is extremely close to the literature values,^{13,14} further verifying that the method and the theoretical model are reliable.

Figure 3 shows the calculated energy-band structures of pure rutile TiO_2 and of the Mo-, Pt-, and Rh-doped systems. As can be seen from Fig. 3(a), the band gap of pure rutile TiO_2 is 1.968 eV, which is less than the experimental value (3.0 eV). The discrepancy is mainly due to the influence of the generalized gradient approximation; however, as an effective approximation, the relative values of the calculated results are very accurate and do not affect the analysis of energy bands and density of states.^{7,8}

Figure 3(b) shows that the bottom of the conduction band moves significantly downward and beyond the Fermi level, and the top of the valence band also moves downwards. Because the

TABLE I. Lattice constants (a , b , $2c$, V , θ , D) of systems before and after doping.

Parameter	R_X	$a/\text{\AA}$	$2c/\text{\AA}$	$V\text{\AA}^3$	$D_{\text{Ti-O}}/\text{\AA}$	$D_{\text{X-O}}/\text{\AA}$	$\theta_{\text{O-Ti-O}}(^{\circ})$
Reference ^a		4.594	5.917				
		4.665	5.947				
Un-doped		4.675	5.925	129.503	1.954		90.000
Mo-doped	2.01	4.708	5.943	131.621	1.992	1.964	89.985
Pt-doped	1.83	4.708	6.029	133.621	1.941	2.069	89.554
Rh-doped	1.83	4.704	6.002	132.805	1.948	2.057	89.780

^aReferences 10 and 11.

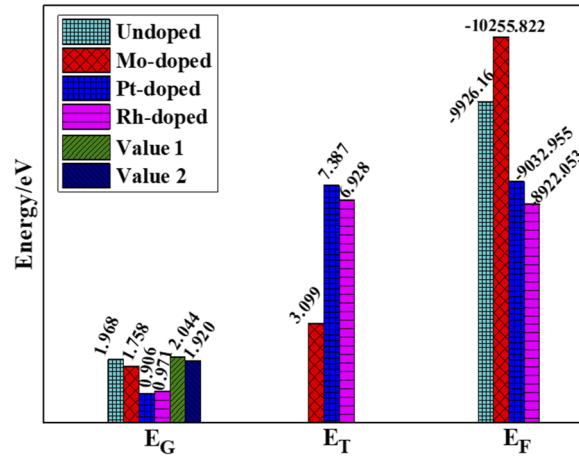


FIG. 2. E_G , E_T , E_F of systems before and after doping (Value 1,¹³ Value 2¹⁴).

conduction band shifts more in energy than does the valence band, the band gap of the system decreases, but this reduction is not significant. Figures 3(c) and 3(d) show that the top of the valence of the Pt- and Rh-doped systems remains almost unchanged, whereas the bottom of the conduction band shifts to lower energy and several impurity levels form near the Fermi level (this is particularly evident in the Rh-doped system). Moreover, parts of the impurity levels thus formed cross the Fermi level, leading to a highly active system. Note that a direct band gap transforms into an indirect band gap in Pt- and Rh-doped systems. Normally, electron transitions can be implemented by the absorption and release of phonons for indirect-band-gap semiconductors. However, absorbing or emitting phonons is

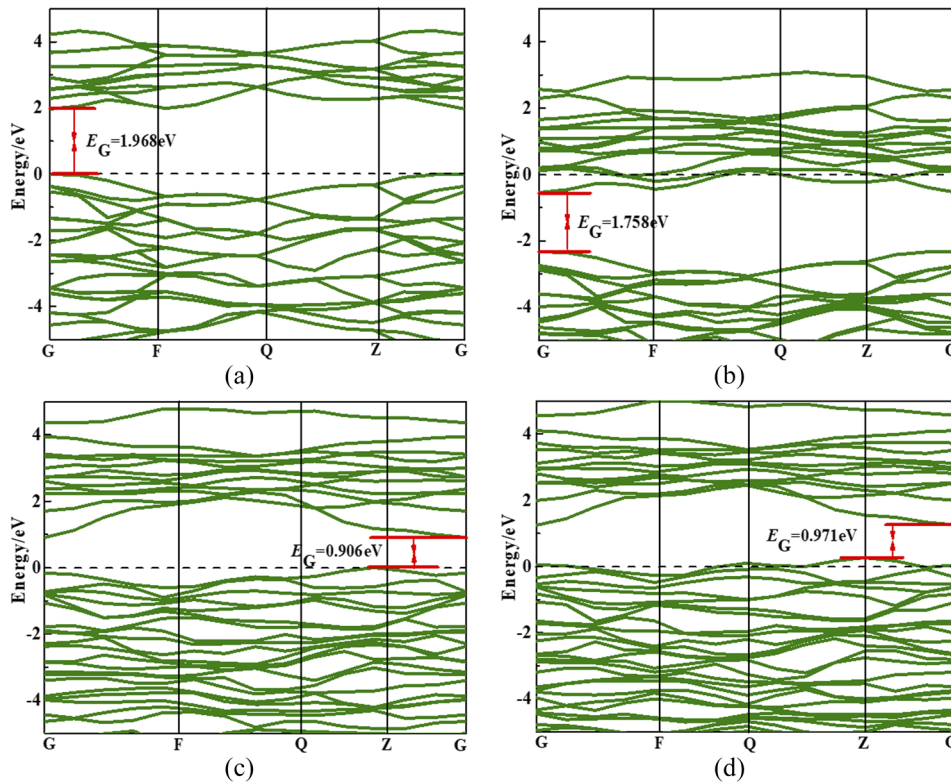


FIG. 3. Band structure of systems before and after doping: (a) undoped, (b) Mo doped, (c) Pt doped, (d) Rh doped.

not required for electron transitions in direct-band-gap semiconductors. Generally speaking, direct-band-gap semiconductors are commonly used as luminescent materials whereas indirect-band-gap semiconductors serve as photoelectric detectors for diodes and photovoltaic devices for solar cells, but cannot be used as light-emitting devices.

C. Density of states

Figure 4 shows the total density of states (DOS) and the partial density of states (PDOS) of pure rutile TiO₂ and doped TiO₂, taking the Fermi energy as zero. Six peaks appear in the DOS of pure rutile TiO₂. From low-energy to high-energy, the six peaks originate from (i) Ti *s*, Ti *p*, O *s*, O *p*, (ii) Ti *d*, O *p*, and (iii) Ti *d*, O *p*, and Ti *d* orbital electrons. The three peaks near the Fermi level are dominated by O *p* and Ti *d* orbital electrons, indicating that the O *p* and Ti *d* orbital electrons form an impurity level near the Fermi level, which facilitates the passage of electrons across the band gap into the conduction band. However, due to the limited contribution of Ti *d* electrons, the energy of the impurity level is very small, so pure rutile TiO₂ is a wide-band-gap semiconductor with a band gap of 2.0 eV.

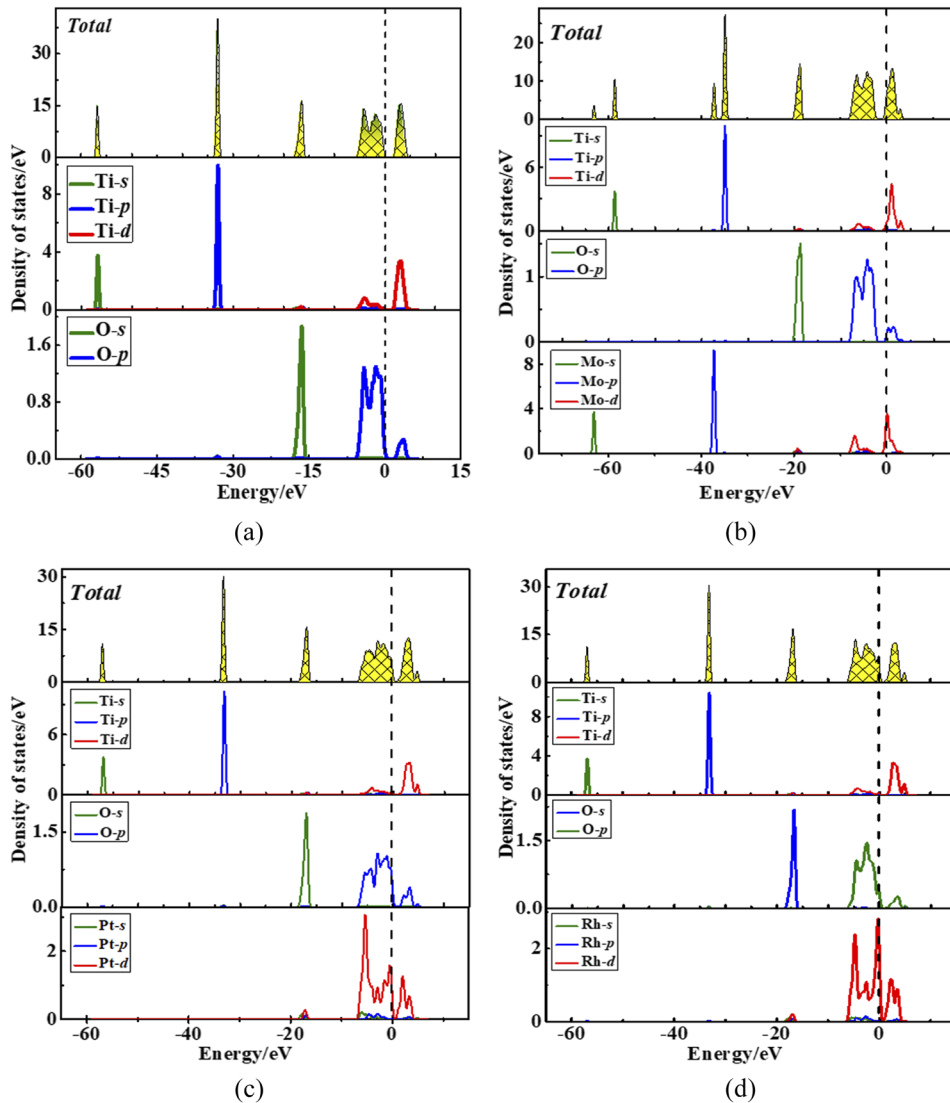


FIG. 4. Density of states of systems before and after doping: (a) undoped, (b) Mo doped, (c) Pt doped, (d) Rh doped.

Figures 4(b)–4(d) show the DOS of doped systems. A peak in the DOS is present in the region of -30 to -40 eV because of the introduction of Mo p orbital electrons in the Mo-doped system, which facilitate the movement of low-energy electrons located in the range of -40 to -30 eV. Furthermore, the DOS peak near the Fermi level comes from the joint action of Ti d , O p , and Mo d orbital electrons, forming the impurity level, but it has no obvious effect on reducing the band gap of the system because of the weaker effect of the Mo d orbital. However, since Pt and Rh atoms possess abundant d orbital electrons, the Pt d and Rh d orbital electrons make a significant contribution to the DOS peaks near the Fermi energy, forming a number of impurity levels, which facilitates the movement of electrons across the Fermi energy into the conduction band, thereby improving the electrical conductivity of Pt- and Rh-doped systems.

D. Charge-difference density

To further explore the electronic structure of pure rutile TiO_2 and doped systems, Fig. 5 shows the calculated charge-difference density. The charge-difference density caused by doping depends strongly on the type of dopant, with the different dopants causing different effects. The blue areas represent electron deficiency, and the red areas represent electron enrichment. According to Fig. 5(a), Ti atoms are surrounded by small blue areas, which indicate that the covalence is extremely weak in the region around the Ti atoms whereas the ionic character is very strong. “Heart-shaped” red areas

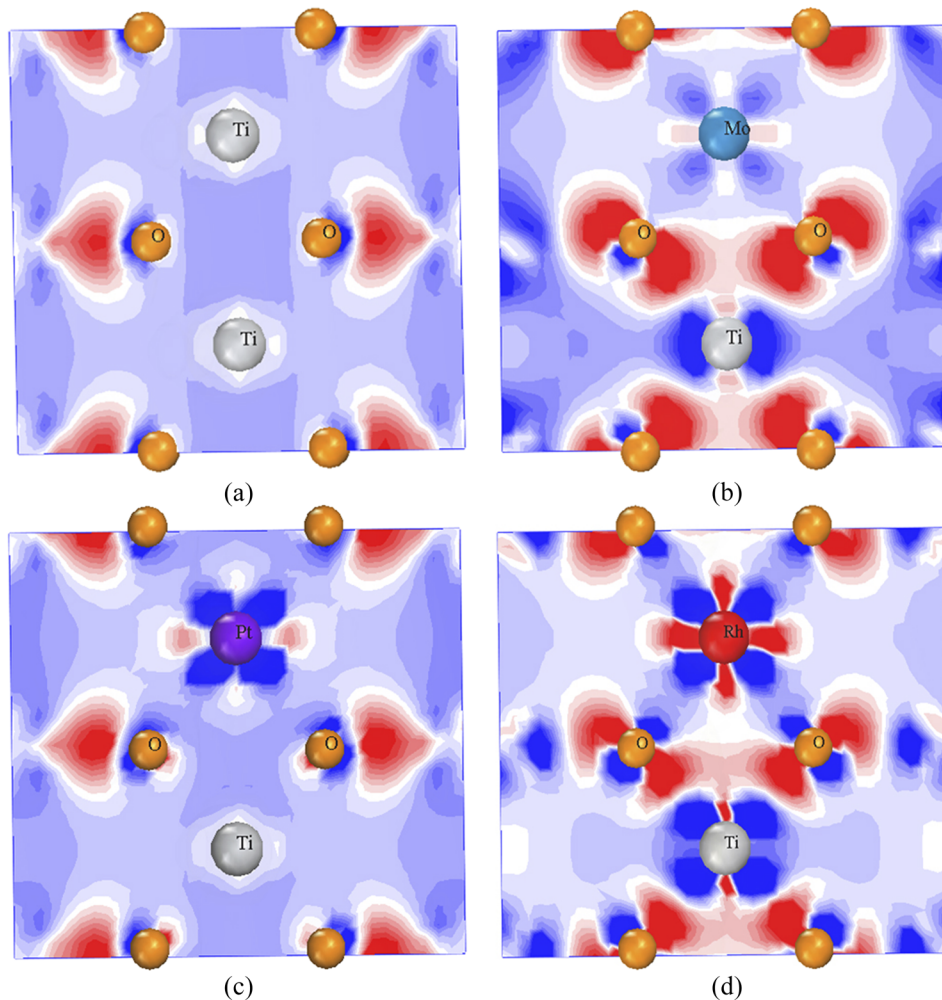


FIG. 5. Charge difference density of systems before and after doping: (a) undoped, (b) Mo doped, (c) Pt doped, (d) Rh doped.

TABLE II. Population of bonds before and after doping.

Parameter	Ti–O		R–O	O–O
Undoped	0.39	0.39		–0.06
Mo doped	0.35	0.27	0.42	–0.04
Pt doped	0.33	0.27	0.28	–0.04
Rh doped	0.34	0.29	0.27	–0.06

appear mostly around O atoms, with small electron-deficient areas, which means an extremely strong ionic character around the O atoms.

Figure 5(b) shows the charge-difference density map for the Mo-doped system, which shows a large “four-petal-shaped” electron-deficient area around the Mo atom, whereas a “crescent-shaped” electron-enrichment area appears around the O atoms, implying that the electron enrichment in the vicinity of the N atom changes and the inhomogeneity of the electron cloud distribution in the system increases. Conversely, upon Mo doping, the charge distribution around the Ti atom also changes significantly. A certain range of electrons are missing around the Ti atom and the degree of electron enrichment around the O atoms in the direction of bonding with Ti is weakened, indicating that Mo doping increases the covalence in the region around the Ti atom.

As shown in Figs. 5(c) and 5(d), electron enrichment occurs around the Pt and Rh atoms, indicating a weakened covalence. The red region near the Rh atom is larger so the ionic character is stronger. Also, an interaction occurs between the electron-enriched and electron-deficient areas, similar to the “petal” shape around the Rh atom. Meanwhile, the electron-deficient area around the Ti atom grows, although the electron enrichment of O in the direction of bonding with Ti is weakened, meaning that the covalent bonding between Ti and O atom is weakened.

The population refers to the distribution of electrons within various atomic orbitals, so a deep understanding of the bonding of atoms in a molecule may be had by analyzing the calculated population. Generally, a large population indicates stronger covalent interactions, whereas a small population indicates stronger ionic interactions.^{15,16} As shown in Table II, the covalence of Ti–O bonds in the system are weakened upon doping with Mo, Pt, and Rh, and the population of new bonds formed between dopants (Mo, Pt, Rh) and O atoms is 0.42, 0.28, and 0.27, respectively, showing that the Mo–O bond is the most covalent, which is consistent with the results of the analysis of the charge-difference density.

E. Optical properties

1. Absorption spectra

The absorption coefficient is the percent attenuation of light intensity per unit propagation distance in the medium.^{17,18} Figure 6(a) shows that the strongest absorption peak ($5.235 \times 10^5 \text{ cm}^{-1}$) for pure rutile TiO_2 is at 36.597 eV, and the peak is greatly reduced and redshifted upon doping. The maximum absorption peaks of Mo-, Pt-, and Rh-doped systems are 3.879×10^5 , 4.089×10^5 , and $4.094 \times 10^5 \text{ cm}^{-1}$, respectively (or 36.327, 36.557, and 36.594 eV), and gradually decrease with increasing photon energy. In addition, a dwarf absorption peak appears in the low-energy region, but far from the peak at 36 eV, indicating that the system absorbs short wavelengths much more strongly than long wavelengths.

Figures 6(b)–6(e) show the absorption spectra in three different polarization directions: [100], [010], and [001], for pure rutile TiO_2 and the three doped systems. The total absorption spectra of the pure and doped systems are very similar in all three polarization directions, which reflects the isotropy of the crystal.

2. Dielectric constant

As shown in Fig. 7(a), the static dielectric constant of the pure rutile TiO_2 system is 5.790 eV, and the real part increases with the increasing energy in the low-energy region. The maximum 9.912 is at 2.519 eV and decreases sharply with increasing photon energy to reach a minimum at about 7.537 eV.

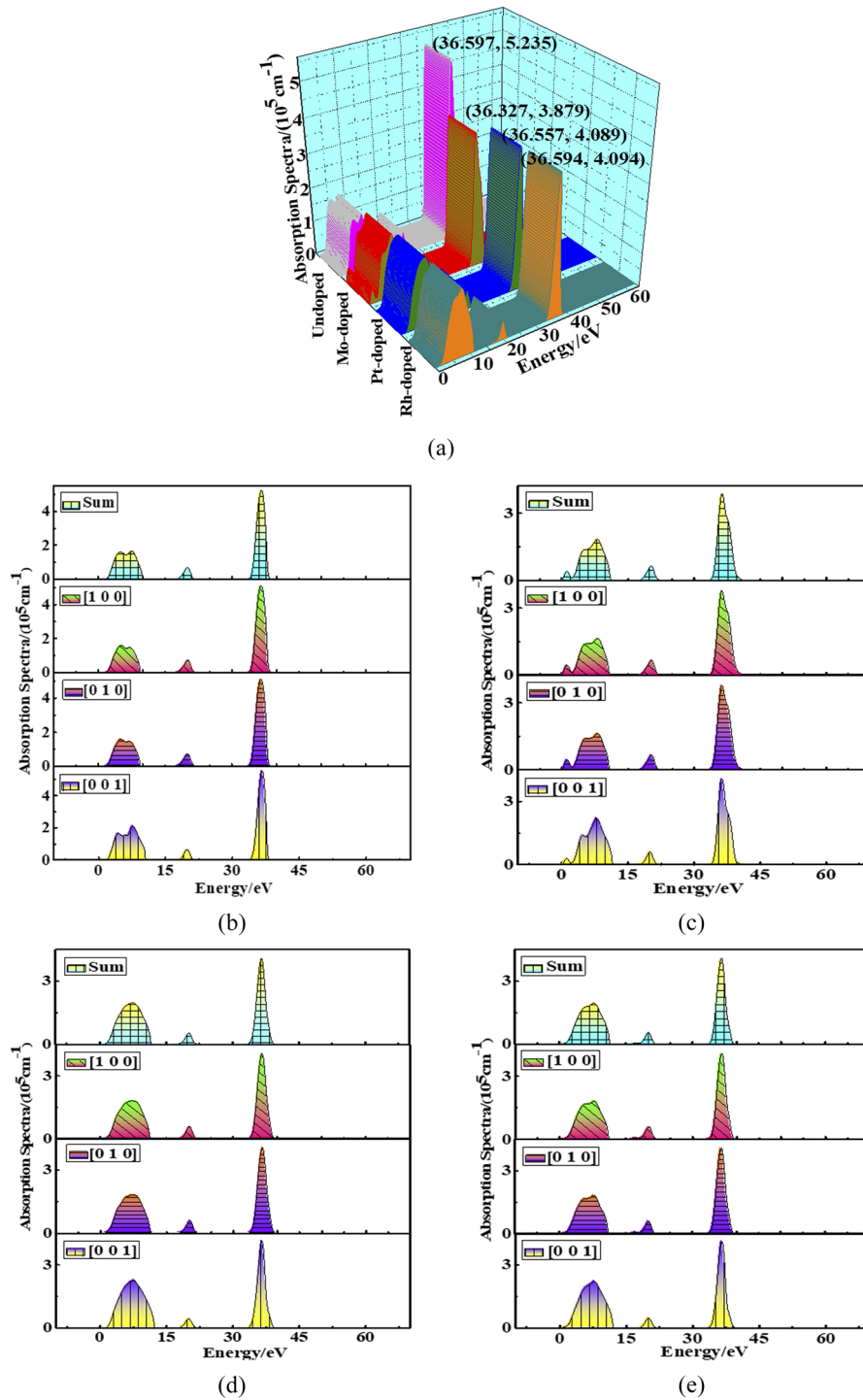


FIG. 6. Absorption spectra of (a) systems before and after doping and (b)–(e) in three different polarization directions: [100], [010], [001].

Upon doping with Mo, Pt, or Rh, the static dielectric constant of the system increases significantly by 72.698, 7.648, and 9.903, respectively.

Figure 7(b) shows the imaginary part of the pure rutile TiO_2 and the doping system. The imaginary part of the dielectric constant of the undoped, Mo-, Pt-, and Rh-doped systems has a second peak at 19.892, 20.091, 20.053, and 19.994 eV, respectively. The imaginary part gradually decreases with

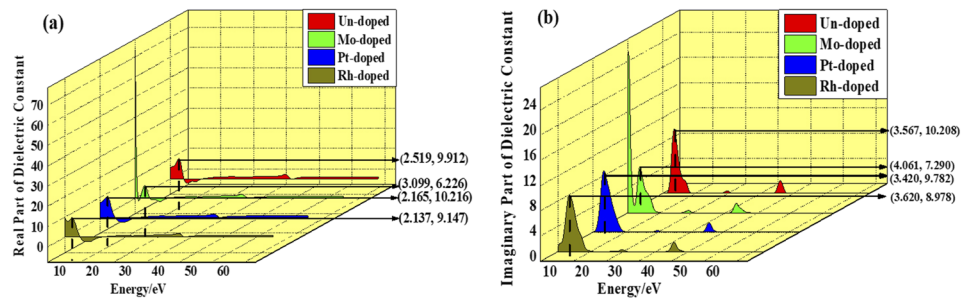


FIG. 7. (a) Real part of dielectric constant of systems before and after doping. (b) Imaginary part of dielectric constant of systems before and after doping.

increasing photon energy and a third peak appears at about 36 eV. This third peak is due to interband transitions, which mainly originates from the d orbital electrons of the dopants. The imaginary part eventually goes to zero as the photon energy continues to increase. The Rh- and Pt-doped systems have lower static permittivity and dielectric loss. In the Mo-doped system, the magnitude of the host peak of the imaginary part of the dielectric constant located at 4.061 eV is 7.290. Compared with the pure system and other doped systems, the peak in the imaginary part of the dielectric constant of the Mo doping system is the smallest, although the peak at 0 eV is the highest.

Above all, lower dielectric loss occurs in the low-energy region for Pt- and Rh-doped systems, which leads to a superior service life as dielectric materials and is conducive to applications of dielectric materials.

IV. CONCLUSIONS

In summary, we use the CASTEP module based on density functional theory to calculate and analyze the electronic structure and optical properties of pure rutile TiO_2 and Mo-, Pt-, and Rh-doped systems. The main results are as follows:

- (1) Due to the numerous d orbital electrons of Mo, Pt, and Rh, they hybridize with Op orbital electrons, forming a different degree of hybrid energy, which increases the electrical conductivity of the system.
- (2) The population of the Ti–O bond decreases upon doping with Mo, Pt, or Rh, indicating that the covalence of the Ti–O bond decreases. Simultaneously, the population of new bonds formed between dopants (Mo, Pt, Rh) and O atoms are 0.42, 0.28, and 0.27, respectively, so ranking the covalent strength of the bonds between the dopants and O gives Mo–O > Pt–O = Rh–O.
- (3) Upon doping, the peak of the absorption coefficient of the host system decreases sharply and redshifts.
- (4) Rh- and Pt-doped systems have lower static dielectric constant and dielectric loss, whereas Mo doping significantly increases the static dielectric constant, which reduces the service life of the material when used as a dielectric. Doping with Rh or Pt reduces the band gap, and the lower dielectric constant and dielectric loss in the low-energy region are more conducive to applications as dielectric materials.

ACKNOWLEDGMENTS

The work was supported by the National Natural Science Foundation of China (51662026, 51561020), the China Postdoctoral Science Foundation (2015M572615, 2016T90959), the Gansu Provincial Youth Science and Technology Fund Projects (1606RJZA157, 1610RJZA005, 1610RJZA014), the Joint fund between Shenyang National Laboratory for Materials Science and State Key Laboratory of Advanced Processing and Recycling of Nonferrous Metals (18LHPY001), and the open fund of the State Key Laboratory of Advanced Processing and Recycling of Non-ferrous Metals.

- ¹ F. Z. Jiang, L. Yang, D. L. Zhou, G. He, J. B. Zhou, F. H. Wang, and Z. G. Chen, *Appl. Surf. Sci.* **436**, 989 (2018).
- ² Q. Y. Hou, Y. Zhang, and T. Zhang, *Acta Optica Sin.* **28**, 1348 (2008).
- ³ J. Reintjes and M. B. Schultz, *J. Appl. Phys.* **39**, 5254 (1968).
- ⁴ A. R. Zanatta, *AIP Adv.* **7**, 075201 (2017).
- ⁵ Q. Y. Hou, Y. Zhang, and T. Zhang, *Acta Phys. Sin.* **57**, 1862 (2008).
- ⁶ Y. L. Liang, S. Y. Dai, X. Q. Fang, and L. H. Hu, *Acta Phys. Sin.* **57**, 1956 (2008).
- ⁷ G. H. Wu, S. K. Zheng, L. Liu, and C. J. Jia, *Acta Phys. Sin.* **61**, 223101 (2012).
- ⁸ Y. Wang, Q. Feng, W. H. Wang, and Y. X. Yue, *Acta Phys. Sin.* **61**, 193102 (2012).
- ⁹ L. Xu, C. Q. Tang, L. Dai, D. H. Tang, and X. G. Ma, *Acta Phys. Sin.* **56**, 1049 (2007).
- ¹⁰ F. C. Pan, X. L. Lin, and H. M. Chen, *Acta Phys. Sin.* **64**, 224218 (2015).
- ¹¹ M. Saini, M. Kumar, and T. Som, *Appl. Surf. Sci.* **418**, 302 (2017).
- ¹² L. J. Chen, W. X. Li, J. F. Dai, and Q. Wang, *Acta Phys. Sin.* **63**, 196101 (2014).
- ¹³ Z. Xie, X. X. Liu, P. Zhan, W. P. Wang, and Z. J. Zhang, *AIP Adv.* **3**, 13211 (2013).
- ¹⁴ Q. Y. Hou and C. W. Zhao, *J. Funct. Mater.* **42**, 783 (2011).
- ¹⁵ K. Chen, G. H. Fan, and Y. Zhang, *Acta Phys. Sin.* **57**, 1055 (2015).
- ¹⁶ X. Y. Hu, H. W. Tian, L. J. Song, P. W. Zhu, and L. Qiao, *Acta Phys. Sin.* **61**, 047102 (2012).
- ¹⁷ Z. Z. Zhang, Q. Y. Hou, and C. Li, *Acta Phys. Sin.* **61**, 117102 (2012).
- ¹⁸ L. Zhang, H. Z. Chen, S. Feng, L. X. Li, Y. K. Li, and J. Y. Chen, *AIP Adv.* **7**, 115021 (2017).